

NANOMATERIALS-BASED THERANOSTIC PLATFORM FOR CANCER TREATMENT USING ULTRASONIC HYPERTHERMIA



By

Ali Hassan

Fiza Khan

Hassan Ahmed

**School of Chemical and Materials Engineering
National University of Sciences and Technology**

2024

NANOMATERIALS-BASED THERANOSTIC PLATFORM FOR CANCER TREATMENT USING ULTRASONIC HYPERTHERMIA



By

Leader - 338640 Ali Hassan

Member-1 - 333804 Fiza Khan

Member-2 - 339913 Hassan Ahmed

A THESIS

Submitted to

National University of Sciences and Technology

in partial fulfilment of the requirements for the degree of

B.E. METALLURGY AND MATERIALS ENGINEERING

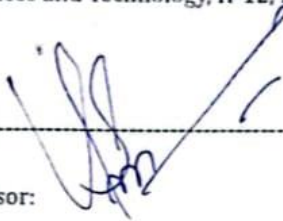
School of Chemical and Materials Engineering (SCME)

National University of Sciences and Technology (NUST)

June 2024

CERTIFICATE

This is to certify that work in this thesis has been completed by **Mr. Ali Hassan, Ms. Fiza Khan, and Mr. Hassan Ahmed** under the supervision of **Dr. Usman Liaqat** and **Dr. Zakir Hussain** at the school of Chemical and Materials Engineering (SCME), National University of Sciences and Technology, H-12, Islamabad, Pakistan.



Advisor:

Dr. Usman Liaqat

Department of Materials Engineering
School of Chemical and Materials
Engineering
National University of Sciences and
Technology

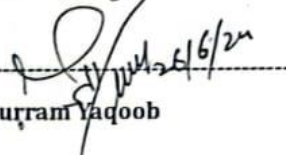


Co-Advisor

Dr. Zakir Hussain

Department of Materials Engineering
School of Chemical and Materials
Engineering
National University of Sciences and
Technology

Submitted Through:

HOD-----

Dr. Khuram Yaqoob

Department of Materials Engineering
School of Chemical and Materials
Engineering
National University of Sciences and
Technology

Principal-----

Dr. Umair Manzoor

Department of Materials Engineering
School of Chemical and Materials
Engineering
National University of Sciences and
Technology

ABSTRACT

Cancer is amongst the most complex global health issues which continues to demand serious action. Several treatments including chemotherapy, radiotherapy, and surgery are being practiced but they have multiple limitations. The side effects of these therapies include the death of healthy cells ultimately resulting in hair loss, nail damage, and skin burns. Nanotechnology has played a crucial role in tackling these issues and nanomaterials-based ultrasonic hyperthermia bypasses some of these side effects and can treat cancer. In the present study, Magnetite and Cobalt doped magnetite nanoparticles were synthesized via co-precipitation route. Cobalt concentration of $x = 0.7$ was used as maximum magnetization is reported at this amount. Calcination was done to remove moisture and impurities from the samples. These synthesized nanoparticles were characterized by XRD, SEM, EDX, and FTIR for evaluating crystal structure, phase purity, morphology, composition, and functional groups, respectively. The findings confirmed the successful synthesis of magnetite as well as the doping of cobalt via XRD, EDX, and FTIR. SEM results confirmed the spherical morphology for both samples. Agglomeration was also observed due to the magnetic nature of nanoparticles. Furthermore, time-temperature analysis was studied using probe sonication in which a temperature increase of 11°C , from 26°C to 37°C , was observed for all four samples which included (1) De-ionized water and Cobalt doped magnetite nanoparticles, (2) De-ionized water, Cobalt doped magnetite nanoparticles and Bacteria (3) De-ionized water, Cobalt doped magnetite nanoparticles and Rose Bengal (4) De-ionized water, Cobalt doped magnetite nanoparticles, Rose Bengal and Bacteria. Finally, a setup was designed to study the temperature behavior of nanoparticles in response to ultrasound in future.

DEDICATION

This study is wholeheartedly dedicated to our beloved parents, who have been our source of inspiration and gave us strength when we thought of giving up. To the instructors who taught us the knowledge needed to complete this project. To the lab engineers who assisted us in providing technical support whenever it was needed.

ACKNOWLEDGEMENTS

Above all, praise is to Allah Almighty for granting us the knowledge and persistence to complete this project. The completion of this project would not have been possible without the expertise and guidance of Dr. Usman Liaqat, our supervisor, and Dr. Zakir Hussain, our co-supervisor. We would also like to express our gratitude to the lab engineers who provided us with technical support. Finally, a debt of gratitude is owed to each of the post-graduate students who stood with us in our hour of need and assisted us in our project.

TABLE OF CONTENTS

LIST OF FIGURES	vi
LIST OF TABLES.....	vii
CHAPTER 1: INTRODUCTION	1
1.1 Research Objectives:.....	2
1.1.1 Objectives.....	3
CHAPTER 2: LITERATURE REVIEW.....	4
CHAPTER 3: METHODOLOGY	8
3.1 Synthesis Techniques:.....	8
3.1.1 Coprecipitation	8
3.1.2 Hydrothermal.....	9
3.1.3 Sol-Gel.....	9
3.2 Materials Procurement	11
3.3 Co-Precipitation Synthesis of Magnetite:.....	11
3.4 Co-Precipitation Synthesis of Cobalt Doped Magnetite:	12
3.5 Calcination	13
3.6 Synthesis of Nanocomposite	14

CHAPTER 4: CHARACTERIZATION TECHNIQUES	15
4.1 X-Ray Diffraction Techniques (XRD)	15
4.2 Scanning Electron Microscopy (SEM).....	17
4.3 Energy Dispersive X-ray Spectroscopy (EDX)	19
4.4 Fourier-Transform Infrared Spectroscopy (FTIR)	21
4.5 Probe Sonication	22
CHAPTER 5: RESULTS AND DISCUSSION	23
5.1 X-Ray Diffraction Techniques (XRD)	23
5.2 Scanning Electron Microscopy (SEM).....	24
5.2.1 Fe ₃ O ₄	24
5.2.2 Co _{0.7} Fe _{2.7} O ₄	25
5.3 Energy Dispersive X-ray Spectroscopy (EDX)	26
5.3.1 Fe ₃ O ₄	26
5.3.2 Co _{0.7} Fe _{2.7} O ₄	27
5.4 Fourier-Transform Infrared Spectroscopy (FTIR)	28
5.5 Time-Temperature Analysis	29
CONCLUSION.....	32
FUTURE PLANS.....	33
Ultrasonic Hyperthermia Setup	33
Material Procurement and Dimensions.....	33

REFERENCES.....35

LIST OF FIGURES

Figure 1: Magnetite synthesis.....	12
Figure 2: Synthesis of cobalt doped magnetite	12
Figure 3: Calcination cycle	13
Figure 4: Synthesis of nanocomposite	14
Figure 5: Experimental Setup of X-Rays Diffraction (XRD)	16
Figure 6: Debye Scherrer equation for measuring crystallite size	16
Figure 7: Experimental Setup of Scanning Electron Microscopy (SEM).....	18
Figure 8: Experimental Setup of Energy Dispersive X-rays Spectroscopy (EDX) for elemental analysis	20
Figure 9: Experimental Setup of Fourier Transform Infrared Spectroscopy (FTIR)	21
Figure 10: Probe Sonicator.....	22
Figure 11: XRD graphs of Fe_3O_4 (left) and $\text{Co}_{0.7}\text{Fe}_{2.3}\text{O}_4$ (right) prepared by co-precipitation method.....	23
Figure 12: SEM images of Fe_3O_4 at different magnification prepared by co-precipitation method	24
Figure 13: SEM images of $\text{Co}_{0.7}\text{Fe}_{2.3}\text{O}_4$ at different magnification prepared by co-precipitation method.....	25
Figure 14: EDX graph of Fe_3O_4 prepared by co-precipitation method	26
Figure 15: EDX graph of $\text{Co}_{0.7}\text{Fe}_{2.3}\text{O}_4$ prepared by co-precipitation method	27
Figure 16: FTIR graphs of Fe_3O_4 (left) and $\text{Co}_{0.7}\text{Fe}_{2.3}\text{O}_4$ (right) prepared by co-precipitation method.....	28
Figure 17: Time-Temperature graph of different combinations of materials.....	31
Figure 18: UHT Setup from literature	33
Figure 19: Self-designed UHT Setup (a) Front view, (b) Top view	34

LIST OF TABLES

Table 1: Literature review	5
Table 2: Advantages and Disadvantages of Nanoparticles Synthesis using Chemical Methods	10
Table 3: Comparison of 2θ degrees between Fe_3O_4 and $\text{Co}_{0.7}\text{Fe}_{2.3}\text{O}_4$ at same miller indices.....	24
Table 4: Materials and amounts for Time-Temperature Analysis	29
Table 5: Probe Sonication specifications	30

CHAPTER 1

INTRODUCTION

Cancer is one of the most lethal diseases worldwide. Despite being a globally known disease, it is one of the challenging diseases to cure. According to the report published by World Health Organization (WHO) in 2020, cancer was the second leading cause of death in the world, with studies reporting that 1 in every 2 people, born after 1960, will suffer from this condition at some moment of their life [1]. About 20 Million death were recorded, and 9.7 million new cancer cases were reported, and this global burden is expected to be 28.4 million by the end of 2040, a 47% rise in cancer cases [2]. The problem is not solved if it is in its early stages but also there is variability in cancer biochemistry. There are different types of cancer in different types of cells. It is a disease in which the body cells grow uncontrollably and spreads to various parts of the body [3]. It can occur in any part of the body and each body part is composed of millions to trillions of cells. Human cells grow and multiply through the process of cell division, they grow and when they die, new cells take their place. Sometimes, the production of this cycle is affected because of the growth of defected and damaged cells which results in tumor formation [4]. Although, there are certain conventional treatments that can treat cancer but with several side effects [5]. These include chemotherapy, radiotherapy, and surgery. Chemotherapy involves the direct delivery of drugs into the main blood stream. Since, it is not a localized drug delivery, so these drugs not only destroy the cancer cells but also kill the healthy surrounding tissues which results in several side effects including hair loss, nail damage, tissue burning etc [6]. The second conventional method is radiotherapy which involves the use of ionizing radiations and charged particles to kill the cancer cells. This method can also lead to skin problems and healthy tissues damaging [7]. The third conventionally used method is surgery which because of its invasive energy involves the direct physical exposure and removing of tumor from the body. The major problems associated with surgery are incomplete removal of tumor because of the spread of cancer in a large area, also it involves difficulty in transition for patients to become stable [8]. To address these

challenges and side effects, there is an utter need for a new treatment method that bypasses all these side effects and treats cancer more effectively. It is known as Ultrasonic Hyperthermia which involves the use of high energy sound waves that can reach through any part of the body through high spatial accuracy. The high energy sound waves increase the temperature to induce cell death. Ultrasounds do not need any kind of sensitizer to induce sufficient heating, but this process only works after long exposure time. To overcome this, NPs such as gold, silica, magnetite, and graphene oxide are used along with ultrasounds to increase additional scattering and attenuations of the sound waves. This leads to a high temperature rise in the tumor region and energy is dissipated in the surroundings. Moreover, when the tumor temperature rises, it results in expansion of blood vessels which increases the blood flow in the body leading to more hemoglobin production and more oxygen permeability which results in production of Reactive Oxygen Species (ROS) and induces oxidative stress on tumor results in eradication of cancer cells.

1.1 Research Objectives

This research majorly focuses on the synthesis of Magnetite nanoparticles and Cobalt doped magnetite nanoparticles for hyperthermia applications. By taking advantage of biological and magnetic properties of cobalt doped iron oxide nanoparticles they are effectively used to generate heat in the localized region to kill cancerous cells. Cobalt doped iron oxide nanoparticles can actively target the tumor site with the help of ultrasounds applied. These nanoparticles properties are governed by their size and shape as for biomedical application size below 100 nm is desired and narrow size distribution is preferred. Also, the uniform size distribution of these nanoparticles is necessary to have high surface to volume ratio at the nanoscale.

Cobalt belongs to transition elements having several properties which makes it useful in various biomedical applications due to its biocompatibility and nontoxic nature when used in smaller concentrations. Therefore, doping of iron oxide nano particles with cobalt of concentration $x = 0.7$ is to be studied in this research and the aim is to study the combine effect of ultrasound and cobalt doped magnetite nanoparticles to enhance the heating in the tumor region and reduces the exposure time to eradicate cancer cells.

1.1.1 Objectives

The following are the objectives of our research work:

- Synthesis and characterization of Fe_3O_4 nanoparticles and optimization reaction parameters to get desired morphology.
- Doping of synthesized nanoparticles with other nanomaterials to enhance the magnetization properties.
- Studying the effect of ultrasounds on doped Fe_3O_4 nanoparticles for hyperthermia application.

CHAPTER 2

LITERATURE REVIEW

Ultrasonic hyperthermia is a technique in which nanoparticles, within tumor, are exposed to ultrasounds and produce heat. This heat increases the blood flow in the tumor which increases oxygen permeability and produces an unfavorable environment for cancer cells to survive. As per the literature, there should be a temperature increase of 6°C to 10°C more than body temperature for effective cancer cells death [1]. This temperature increase is highly localized and heats the tumor from the inside out. Researchers have used transducers as ultrasounds source with a frequency range of 1MHz to 2MHz and a power density range of 1W/cm² to 2W/cm² [9-15].

Spinel ferrites are materials that are ferromagnetic in nature and are ideal for hyperthermia applications. They exhibit more attenuation and scattering of ultrasound which amplifies the heating effect within tumor. J. Beik et al. compared the temperature increase of gold nanoparticles, nano-graphene oxide, and magnetite nanoparticles in response to ultrasounds. It was found that magnetite nanoparticles demonstrated a temperature increase from 37°C to 44°C in a duration of 10 minutes by continuous ultrasound exposure which lies in the required temperature range [10]. At another place, T. SHALABY et al. used magnetite nanofluid to study the tumor mass inhibition ratio. After treatment of 5mins/day for a total of 14 days, tumor weight inhibition ratio was reduced to 58.42%, 30%, and 7.89% for ultrasound treatment, ultrasound alone and Fe₃O₄ NPs, respectively [16]. This clearly shows the potential of magnetite nanoparticles in ultrasonic hyperthermia. Cobalt doped magnetite has a great potential in ultrasonic hyperthermia due to its high magnetization property. It is to be noted that, in this domain, it has only been used in magnetic hyperthermia. For instance, a paper published in the Royal Society of Chemistry in 2021 showed that the highest saturation magnetization of 71.1 emu g⁻¹ resulted when the atomic weight of cobalt was 0.7 i.e. Co_{0.7}Fe_{2.3}O₄ [17]. A detailed literature review is shown in [table 1](#).

Table 1: Literature review

Topic	Aim of research	Steps involved	Materials and Characterization	Conclusion(s)
<p>(1). Measurements of nanoparticle-enhanced heating from 1 MHz ultrasound in solution and in mice bearing CT26 colon tumors. [10]</p> <p><i>2016-Iran</i></p>	<p>Evaluate and compare the Sono sensitizing potentials of gold nanoparticles (AuNPs), iron oxide nanoparticles (IONPs), and nano-graphene oxide (NGO) in the enhancement of ultrasound-induced heat generation.</p>	<ol style="list-style-type: none"> 1. Nanoparticles were purchased. 2. Characterization was performed. 3. In vitro testing 4. In vivo testing 5. Compare results 	<p>Materials</p> <ol style="list-style-type: none"> 1. Gold NPs 2. Iron oxide NPs 3. Nano-graphene oxide <p>Characterization</p> <ol style="list-style-type: none"> 1. TEM 2. SEM 3. DLS 4. Zeta potential 	<ol style="list-style-type: none"> 1. In this study, Sono sensitizing effects of AuNPs, NGO and IONPs were investigated in vitro and in vivo. 2. Experiments revealed that percentages of increases in temperature elevation rates were 12.5%, 20.4%, and 37.5% for IONPs, NGO, and AuNPs, respectively. Gold NPs shows the most heating rate.
<p>(2). A theranostic nrGO@MSN-ION-PEG Nano carrier was developed to enhance the combination effect of sonodynamic therapy and ultrasound hyperthermia for treating tumor. [11]</p> <p><i>2016-Taiwan</i></p>	<p>Development of a novel Nano carrier, mesoporous silica (MSN) grown on reduced graphene oxide nanosheet (nrGO, as a SHT enhancer) capped with Rose Bengal (RB, a sonosensitizer)-PEG-conjugated iron-oxide nanoparticles (ION) to form nrGO@MSN-ION-PEG RB which exhibit the SDT/SHT combination effect with magnetic navigation functionality to enhance localized accumulation at the target tumor site for</p>	<ol style="list-style-type: none"> 1. Synthesis and characterization 2. Detection of single oxygen generation 3. In vitro cell viability/cell culture 4. In vitro hyperthermia 5. In vivo hyperthermia 6. In vivo imaging with magnetic field 	<p>Materials</p> <p>Mesoporous silica (MSN) grown on reduced graphene oxide (nrGO) capped with Rose Bengal (RB)-PEG-conjugated Fe₃O₄ NPs. nrGO@MSN-ION-PEG-RB</p> <p>Characterization</p> <ol style="list-style-type: none"> 1. TEM 2. FTIR 3. DLS 4. Zeta potential 	<ol style="list-style-type: none"> 1. A theranostic agent, nrGO@MSN-ION-PEG-RB, which was fabricated using nanosized reduced graphene oxide/porous silica nanosheets capped with RB-conjugated iron oxide nanoparticles was developed. 2. Results demonstrate that the use of multifunctional nrGO@MSN-ION-PEG-RB nanocomposites together with FUS and MF might open new approaches to cancer therapy

<p>(3). Gold nanoparticle- induced Sono sensitization enhances the antitumor activity of ultrasound in colon tumors. [13]</p> <p><i>2018-Iran</i></p>	<p>The purpose of the present study is to utilize AuNPs in combination with ultrasound in order to assess the in vivo antitumor efficacy of this strategy on BALB/c mice bearing CT26 colorectal tumor model, and therefore to develop a nanoparticle- assisted ultrasound therapy</p>	<ol style="list-style-type: none"> 1. Material purchase 2. Cell culture 3. Characterization 4. In vivo testing 	<p>Material Au NPs</p> <p>Characterization</p> <ol style="list-style-type: none"> 1. PET 2. TEM 3. DLS 	<ol style="list-style-type: none"> 1. The aim of the present research was to assess the Sono sensitizing effect of AuNPs in vivo. 2. The extensive tumor necrosis without the evidence of relapse during the study span and the extracted radiomic features from the PET images confirmed a potent anticancer efficacy caused by the AuNPs and ultrasound combination.
<p>(4). Combined thermo-chemotherapy of cancer using 1 MHz ultrasound waves and a cisplatin-loaded Sono sensitizing Nano platform in an in vivo study. [14]</p> <p><i>2019-Iran</i></p>	<p>Develop a new combinatorial cancer treatment strategy taking advantage of Sono-sensitizing Nano platforms.</p>	<ol style="list-style-type: none"> 1. Synthesis of ACA (Biomaterial) 2. Induce colon tumor cell line in mice. 3. Inject 8 different combinations of material (Separate + combined) 4. Use of PET imaging to check tumor growth retardation. Use of infrared thermal imaging to observe temperature variations 	<p>Materials ACA Nano platform (Alginate coloaded with cisplatin and gold nanoparticles)</p> <ol style="list-style-type: none"> 1. Core material Gold 2. Drug Cisplatin 3. Coating Alginate <p>Characterization</p> <ol style="list-style-type: none"> 1. PET 2. TEM 3. DLS 4. Zeta potential 	<ol style="list-style-type: none"> 1. Researchers used 1 MHz ultrasound waves in combination with a nano platform made of alginate coloaded with cisplatin (as the anti-tumor drug) and AuNPs (as a Sono sensitizing agent) 2. A considerable tumor growth suppression and significant decrease in metabolic activity of tumor cells (obtained from the PET imaging studies) confirmed a potent anti-tumor efficacy caused by the ACA nano platform and ultrasound combination.

		MRI analysis	Characterization 1. TEM 2. Tunable pulse resistive sensing 3. Calibration particles 4. Atomic absorption spectroscopy 5. Titration	targeting and MRI monitoring was proposed. 2. These liposomes co-encapsulate an anti-vascular disrupting agent in order to starve the tumor and modify its microenvironment. 3. The temperature transition of the lipids composing the liposomes was chosen around 43 °C, which can be achieved by HIFU providing focalized mild hyperthermia.
<p>(5). A promising platform of magnetic Nanofluid and ultrasonic treatment for cancer hyperthermia therapy Invitro And In vivo study. [16]</p> <p><i>2021-Germany, Egypt</i></p>	The main objective of this study was to evaluate the cancer cell-destroying capability of MNPs in combination with ultrasound treatment as an innovative Sono magnetic cancer therapy.	1. Synthesis and characterization of magnetic nanofluid 2. Determining cytotoxicity of EACs with MNPs without ultrasound exposure. 3. Determining the effect of ultrasound on EACs without MNPs. 4. In vivo hyperthermia study 5. Ultrastructure study Determination of tumor mass inhibition ratios	Material Fe ₃ O ₄ Nanofluid Characterization 1. TEM 2. XRD 3. FTIR 4. VSM	1. The presence of MNPs in combination with US exposure was found to enhance the rate of destruction of cancer cells.

METHODOLOGY

3.1 SYNTHESIS TECHNIQUES

Nanoparticles (NPs) can be synthesized by using various techniques depending upon the qualitative accuracy of size, shape, and its structure. These techniques can be divided into three major categories including physical, chemical, and biological methods. In physical methods, nanoparticles are synthesized by using techniques like gas phase deposition, pulse laser ablation, electron beam lithography, and power ball milling techniques. Physical methods are extremely undesirable for synthesizing nanoparticles due to presence of excess impurity, less control over particle size, high energy consumption, and limited application (Not used in sensitive application like electrical, biological application, where desired elements such as size, morphology are needed).

Chemical methods include techniques like co-precipitation, hydrothermal and sol-gel methods. Biological methods include green synthesis of nanoparticles using bacteria fungi or protein extracts. The suitable method is chosen based on desired shape, size, distribution, purity, and quantity of end results. The following are the detail of chemical synthesis methods used commonly for the NPs synthesis which include:

3.1.1 Coprecipitation

The co-precipitation method is a versatile chemical technique for synthesizing nanoparticles. It is the process in which precursors such as Iron (II) and Iron (III) are used as solutes, De-ionized water used as solvent and then after the addition of reducing agent in solution, nanoparticles precipitate out from the solution. While continuous stirring by using magnetic stirrer involves here. It is the simplest, common, and widely used technique for the synthesis of nanoparticles. It includes collective existence of nucleation, growth, and coarsening. Nucleation is the key step in this process. In this technique nanosized particles are precipitated out of a continuous solvent. Change in pH, and amount of reducing agent can be used to control particle size and shape and morphology [\[17\]](#).

3.1.2 Hydrothermal

The hydrothermal method having a unique approach for synthesising nanoparticles. Unlike traditional chemical reaction, hydrothermal method uses high temperature and pressure, reactants are dissolved in a solvent inside of a closed container called an autoclave during this procedure. The vessel is heated above the boiling point of the solvent while operating at high pressure. Since their solubility rises dramatically with temperature, basic solvents are preferred. Here selection of solvent need cares, mostly water use as solvent. Solvent becomes the reaction medium, usually heated to temperature range 100°C to 300°C, boiling point of water exceeding at standard pressure. Moreover, autoclave pressurize the system and create the unique reaction environment by protect water to boil away [\[18\]](#).

This method allows for good control over crystallinity, size, and shape. The process's disadvantages include costly equipment, safety concerns during the reaction, and the potential for an autoclave explosion if not handled correctly.

3.1.3 Sol-Gel

Sol-gel is a process in which solution and gel can be obtained simultaneously as well as separately. Sol can be described as colloidal solution made up of particles suspended in liquid phase whereas gel can be defined as solid macromolecule in a solvent. It is a process which basically involves two steps hydrolysis and polycondensation. The idea behind is to dissolve compounds in a solvent and bring it to back to solid in a controlled manner. This process allows homogeneous mixing at atomic scale. Several products including dense powder, thin films, porous structures, and fibres can be synthesized through this method [\[19\]](#). The pros and cons of these techniques are summarized in [table 2](#).

Table 2: Advantages and Disadvantages of Nanoparticles Synthesis using Chemical Methods

Methods	Advantages	Disadvantages
Co-precipitation	<ul style="list-style-type: none"> • Simple process • Ambient working conditions • Can control particle size 	<ul style="list-style-type: none"> • Reactants with different precipitation rate are difficult to work with in this process. • Impurities may also get precipitated during the reaction.
Hydrothermal	<ul style="list-style-type: none"> • Precise control on size shape, crystallinity, and distribution of final product • Significantly enhanced chemical reactivity of reactants 	<ul style="list-style-type: none"> • Expensive autoclaves required. • Un-safe reaction process
Sol Gel	<ul style="list-style-type: none"> • High purity products • Better control over product final composition • Controlled porosity can be obtained 	<ul style="list-style-type: none"> • Longer reaction time • Harmful organic solvents

3.2 Material Procurement

Precursors salts; Ferrous Sulphate Heptahydrate ($\text{FeSO}_4 \cdot 7\text{H}_2\text{O}$), Ferric Chloride Hexahydrate ($\text{FeCl}_3 \cdot 6\text{H}_2\text{O}$), Cobalt (II) nitrate hexahydrate [$\text{Co}(\text{NO}_3)_2 \cdot 6\text{H}_2\text{O}$], Ammonia (NH_3), Sodium Hydroxide (NaOH), Rose Bengal were purchased from Sigma Aldrich and consumed for synthesis of magnetite nanoparticles, cobalt doped magnetite nanoparticles, and nanocomposite of cobalt doped magnetite nanoparticles Plus Rose Bengal while glassware, spatula, dropper, Magnetic stirrer, Ethanol and De-ionized water were purchased from United Traders. De-ionized water used as solvent for making solution. Ethanol used as purification purpose.

3.3 Coprecipitation Synthesis of Magnetite

Ferrous Sulphate Heptahydrate (Fe^{2+}) and Ferric Chloride Hexahydrate (Fe^{3+}) salts were used as solute for synthesizing magnetite NPs. Both salts were added in separate beaker of 50mL along a magnetic stirrer each on hot plate. It was stirred for 15 minutes after which both solutions were added in single beaker of 100mL. Continuous stirring was given to avoid agglomeration of salts. After stirring for 45 minutes, 5ml Ammonia, as a precipitating agent, was added at a time to control the size of nanoparticles. By this the growth and nucleation of nanoparticles will start at a time which results in narrow size distribution of nanoparticles. Reducing agent raised the pH to 13 and changed the color of solution to black.

After 45 minutes of continuous stirring, solution was poured into the centrifuge tubes to reduce the pH level. Next step was centrifuging for washing the nanoparticles and reducing the pH level from pH 13 to 7. Tubes were placed perpendicular to each other having same weight (measured by weight balance). Solution was washed 3-4 times by de-ionized water at 3000 rpm for 1 hr while continuous pH checking was observed by pH paper. After a 3-4 cycle of centrifuge, pH reduced to 7 from 11. Nanoparticles were placed on a petri dish from centrifuge tubes and ethanol was added to facilitate the evaporation of de-ionized water. After 3-5 minutes, petri dish was placed in a drying oven for 12 hrs at 60°C to remove moisture. After 12 hrs, nanoparticles become completely dry. After drying, nanoparticles were grinded in mortar pestle to achieve good morphology and better SEM

results. After 20 minutes of continuous grinding in the Mortar pestle, the desired nanoparticles were achieved successfully. Synthesis of magnetite is shown in [figure 1](#).

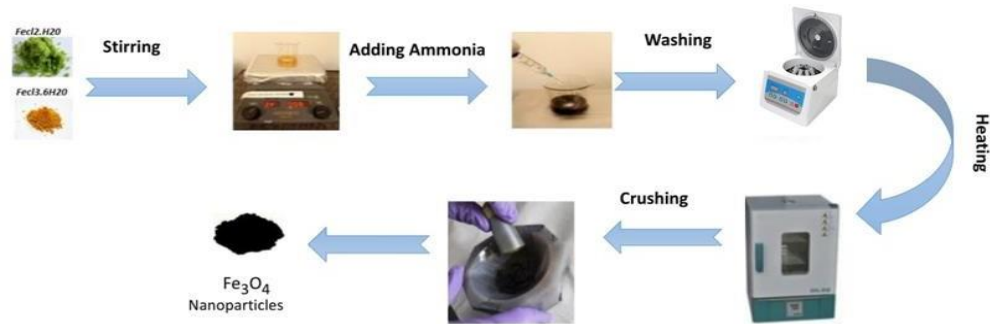


Figure 1: Magnetite synthesis [20]

3.4 Coprecipitation Synthesis of Cobalt Doped Magnetite

Synthesis of cobalt doped magnetite was almost similar to the synthesis of magnetite nanoparticles except for some variations in parameters like time, temperature, rpm, and salts. [Figure 2](#) demonstrates the complete process. Cobalt nitrate was used as a Co^{2+} salt along with Fe salts as solute, De-ionized water used as solvent and sodium Hydroxide (NaOH) was used as reducing agent instead of Ammonia (NH_3) to precipitate out the nanoparticles from solution.

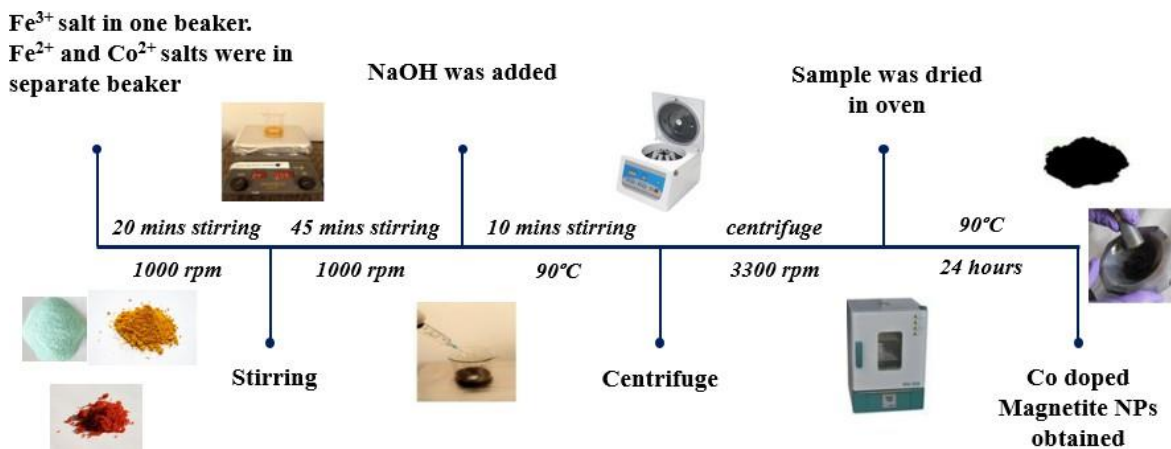


Figure 2: Synthesis of cobalt doped magnetite [21]

3.5 Calcination

Calcination was done for magnetite nanoparticles. In this process, oxygen environment was given to nanoparticles to modify and enhance the properties of nanoparticles such as to get better size, crystal structure and phase. Calcination also resulted in elimination of the impurities, and moisture content from nanoparticles. Under oxygen environment, the nanoparticles were placed at 300°C for 4 hrs while an additional 1 hr was given to reach 300°C. After this, the sample was Furnace cooled and magnetite sample obtained. Calcination cycle is shown is [figure 3](#) below.

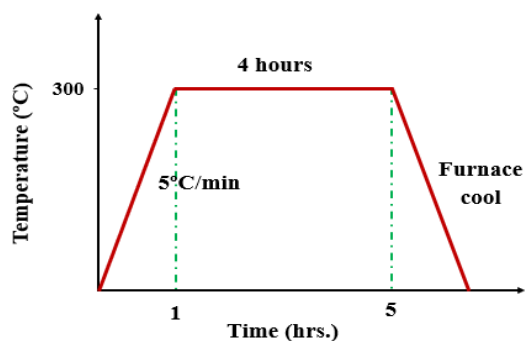


Figure 3: Calcination cycle [\[22\]](#)

3.6 Synthesis of Nanocomposite

In order to enhance the effectiveness of ultrasonic hyperthermia, nanomaterials known as Sonosensitizers were used and combined with cobalt doped magnetite nanoparticles. The name of the sonosensitizers is Rose Bengal which is reported to be used in this domain of treatment [14]. It was procured from Sigma-Aldrich. Upon interaction with ultrasounds, Rose Bengal generates Reactive Oxygen Species (ROS) which induces oxidative stress on tumor from within.

A nanocomposite of cobalt doped magnetite nanoparticles and Rose Bengal was prepared by first adding 0.03 grams of nanoparticles in 20 ml de-ionized water. After stirring 10 minutes, Rose Bengal with the same amount was added and the solution was kept on stirring at 1000 rpm for 30 minutes. No heating was provided during the process. The flow diagram of the process can be seen below in figure 4.

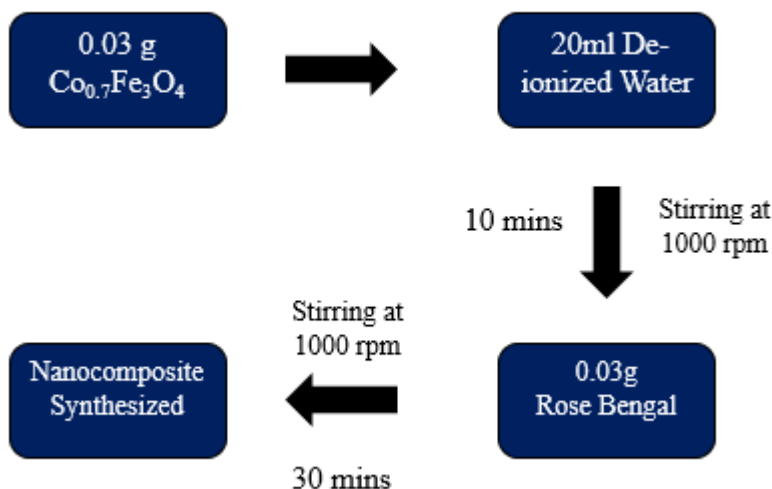


Figure 4: Synthesis of nanocomposite

CHARACTERIZATION TECHNIQUES

Magnetic nanoparticles are classified as important class of materials characterized by their significant magnetic properties and their smaller size such as, less than 100nm. To determine the size, morphology, crystallography of magnetite nanoparticles various techniques used.

4.1 X-Ray Diffraction Techniques

X-ray diffraction is the non-destructive and powerful technique to determine the crystal structure, phase identification, and crystallite size of unknown sample. Its working principle is the beam of X-rays from the source are directed towards the powdered sample. X-rays interact with the crystal lattice of sample and diffracted from the sample to the detector at the specific pattern. Every materials structure has a unique diffraction pattern so we can say that diffraction pattern act as fingerprint. Detectors measure the angle and intensity at which x-rays diffracted from the samples lattice. By these measuring, crystal structure of sample are measured [23]. An experimental setup of XRD is shown in [figure 5](#).

To find the crystal structure and phase identification of magnetite, first step of XRD is sample preparation. Sample is prepared in powdered form to ensure penetration of x-rays beam onto the sample and then diffracted x-rays can be detected accurately. Then x-rays analysis is performed by using an X-ray diffractometer. The diffracted x-rays pattern is collected from the sample as a function of angle, measured as a diffracted angle (2θ). The range lies in between 0° to 80° . Then diffracted pattern analyse by using software to identify of peaks. These peaks correspond to diffracted x-rays patterns that are scattered by sample. There is reference database exist for comparing the peaks and matched with the known positions and intensity for identification of peaks. At last, intensity and position of peaks with respect to angles are used to determine the crystal structure of sample [24].

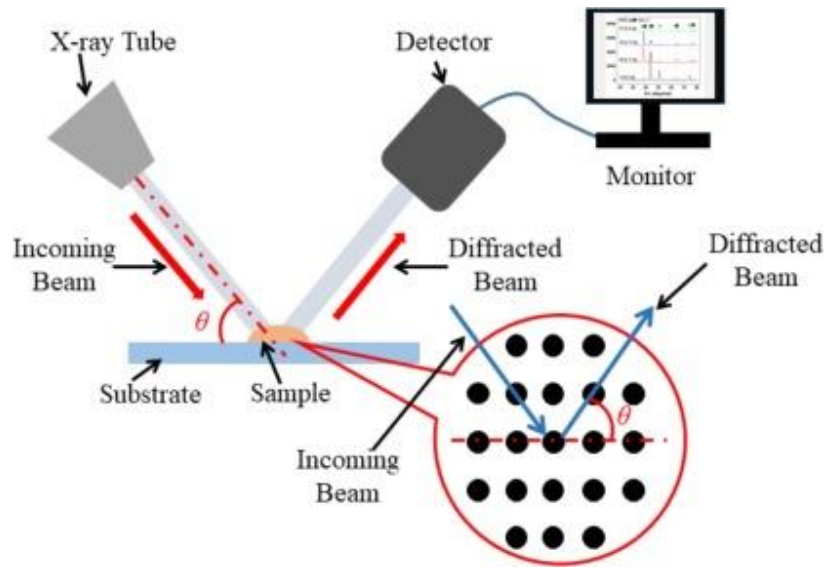


Figure 5: Experimental Setup of X-Rays Diffraction (XRD) [25]

Small quantity powder of nanoparticles is taken and analysed through XRD at angle 0° to 80° at the step size of 0.04 for 50 minutes. For phase identification, results obtained from this scan is taken and compared with reference JCPD file. Crystallite size of nanoparticles can be obtained by using [Debye Scherrer equation](#).

$$D = \frac{K\lambda}{\beta \cos \theta}$$

Figure 6: Debye Scherrer equation for measuring crystallite size [26]

Where is the D crystallite size in nm, K is the Scherrer constant, λ is the wavelength of diffracted x-rays, β is the full width at half maximum (FWHM) of the peak, and θ is the diffraction angle.

4.2 Scanning Electron Microscopy

Scanning Electron Microscopy (SEM) is also a non-destructive technique used to analyse the morphology, topography, orientation and chemical composition of conductive sample. The Scanning electron microscopy (SEM) consists of an Electron gun use as a source of high energy electrons, a sample holder at which sample is placed, and a detector that measure the signal that came from the interaction of electron with the sample surface [\[27\]](#).

It works by directing the high energy electron beam towards the sample surface, this high energy electron beam interacts with the sample surface and generated the signal which is used to create a high-resolution image of samples surface. The SEM consisting of Electron gun a source of high energy electrons, a sample holder at which sample is placed, and a detector that measure the signal that came from the interaction of electron with the sample surface. An experimental setup of SEM is shown in [figure 7](#).

Various signal generated through the interaction of high energy electron with sample surface Includes, Secondary electron (low-energy electrons used to analyse the topographic information), Auger electron (High-energy electron used to analyse the chemical composition), Backscattered electron (high-energy electrons used for chemical composition and surface topography information) etc. These signals detected by detector and used to generate the image of sample surface [\[28\]](#).

In case of magnetite nanoparticle sample, SEM can provide the information of size, shape, and surface features of magnetite nanoparticle. As high vacuum is required for SEM so results can vary or depends upon the source and operating conditions. Higher the vacuum level higher the resolution of image due to less scattering of electron by gas molecules.

Furthermore, scanning electron microscope (SEM) can also be coupled Energy-dispersive spectroscopy (EDX) to measure the elemental composition of sample. After scanning the surface of sample, data is collected as a function of position of electron beam which is in x and y coordinates. The image is generated by mapping the intensity of incoming signals from samples surface.

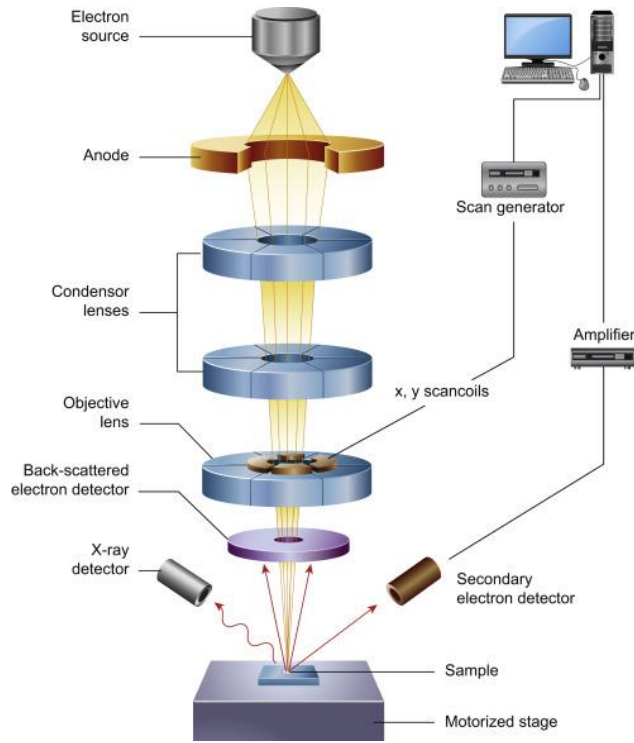


Figure 7: Experimental Setup of Scanning Electron Microscopy (SEM) [29]

Different Images can be taken at different resolution using acceleration voltage of 20kV to analyse the sample accurately.

4.3 Energy Dispersive X-ray Spectroscopy (EDX)

Energy Dispersive X-rays Spectroscopy (EDX) serve as interconnected or supplemental technique to Scanning electron microscopy (SEM). Unlike SEM's used to analyse morphology, EDX used to analyse the elemental composition of powdered sample.

Its working is like that, High energy electron beam interact the sample and excites its atom when atom becomes stable, they release X-rays of unique Energy. Detectors capture these X-rays and convert their energy into electrical signals. Then software generates the X-rays spectrum by analysing these signals and this generated X-rays spectrum reveals the elemental composition. The peaks coming from spectrum corresponds to the presence of elements [30]. An experimental setup of EDX is shown in [figure 8](#).

In case of magnetite sample (Fe_3O_4), there will be distinct peaks for iron (Fe) and oxygen (O) which confirms magnetite composition. In this qualitative analysis of magnetite shows that, the atomic percent of oxygen is more than that of iron which corresponds to the original ratios of oxygen and iron in the magnetite formula,

While the intensity of peaks indicates the relative abundance of each element. There will be some limitation while performing this technique is that it gives a semi-quantitative result. By using EDX we can find the expected stoichiometry of magnetite sample. While advanced EDX system can create elemental maps by collecting x-rays spectra from different points of sample surface. This helps us to identify the variations in composition within the different regions of sample. EDX is a non-destructive technique it means it does not cause volume loss hence same sample can be tested again and again [31].

We can get visual and compositional information of sample by coupling EDX and SEM. SEM produces detailed images while the EDX provides elemental composition of sample. This coupling is powerful for sample characterization, allowing us to relate the microstructure with composition of sample.

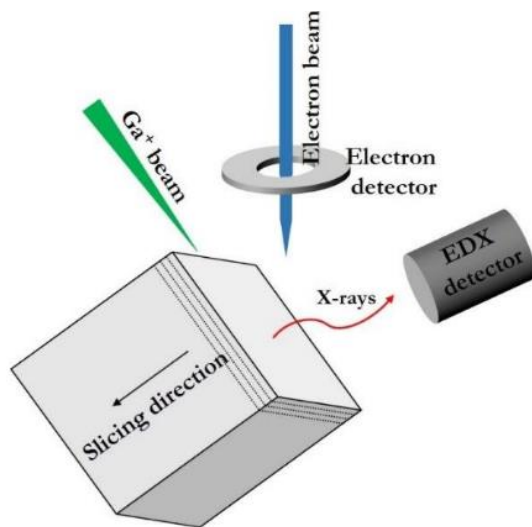


Figure 8: Experimental Setup of Energy Dispersive X-rays Spectroscopy (EDX) for elemental analysis [\[32\]](#)

The elemental composition of magnetite samples determined by EDX analysis. EDX provides detailed information about concentration of elements.

4.4 Fourier-transform infrared spectroscopy (FTIR):

Fourier Transform Infrared (FTIR) spectroscopy works on the principle of Infrared rays absorb by the materials to analysis the chemical composition and functional groups of samples. The FTIR spectrometer consists of IR source, sample stage and a detector. In this, sample should be in fine powdered or in thin film form to ensure that infrared radiation can effectively interact with sample. When IR radiations interact with sample molecules, these molecules absorb certain infrared wavelength while remaining rays are transmitted and measured. FTIR technique is used to determination of functional groups present on surface of sample.

In FTIR (Fourier Transform Infrared Spectroscopy), a plot of the intensity of transmitted light as a function of wavenumber is obtained. This technique operates in the range of 4000 cm^{-1} to 400 cm^{-1} using infrared rays from the spectrometer. Each peak in the spectrum corresponds to a specific functional group. In the case of magnetite nanoparticles, the peaks arise from Fe-O bond stretching. We can identify the functional groups of magnetite samples by comparing the obtained spectrum with reference spectra [33].

The position and intensity of the peaks indicate the surrounding chemical environment. If a shift in the peak is observed, it suggests variations in the iron's oxidation state within the magnetite lattice. FTIR can also detect impurities in the sample, which would appear as additional peaks in the spectrum. The experiment setup required for FTIR are shown in [figure 9](#).

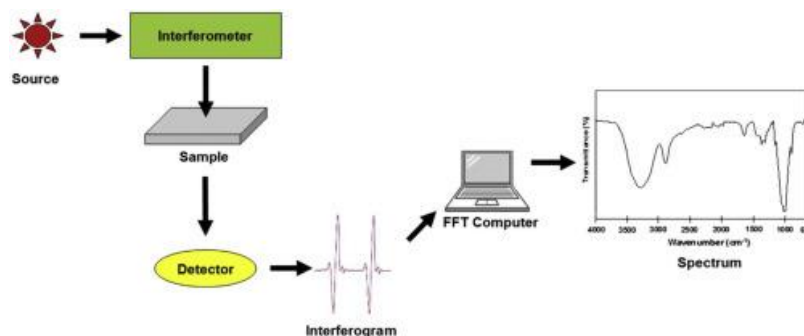


Figure 9: Experimental Setup of Fourier Transform Infrared Spectroscopy [34]

4.5 Probe Sonication

Probe sonication works in the principle of directing high-frequency ultrasound waves at the sample through probe to agitate sample particles. Its working is ultrasonic convertor or generator converts the electrical energy into high frequency sound waves in the range of 20 kHz to 40 kHz. These sound waves propagate through the liquid medium.

Then ultrasound waves are transmitted through probe while probe tip is immersed in the liquid medium. The ultrasound waves propagate through the liquid medium. This probe tip vibrating at high frequency and creates vibrations in liquid medium and creates small bubbles. When these bubbles collapse, it releases energy in form of wave. This phenomenon known as cavitation; it generates localized high temperature and pressure and produce shear force. As they are localized so they create high-pressure zone and low-pressure zone. The tiny bubbles rapidly formed and collapse in low-pressure zone [35].



Figure 10: Probe Sonicator

A common Probe Sonicator is shown in [figure 10](#). It uses in various applications including nanotechnology, biotechnology, material science, environmental science etc. In case of magnetite nanoparticles, through probe sonicator the relation of ultrasounds with nanoparticles can be analyse by considering temperature as a function time.

RESULTS AND DISCUSSION

5.1 X-Ray Diffraction Techniques (XRD)

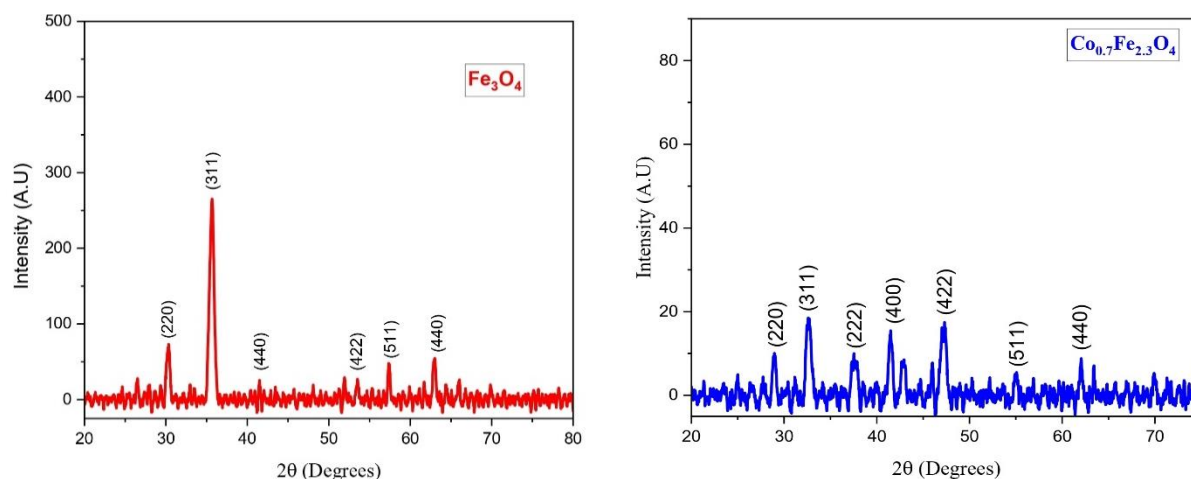


Figure 11: XRD graphs of Fe_3O_4 (left), $\text{Co}_{0.7}\text{Fe}_{2.3}\text{O}_4$ (right) prepared by co-precipitation method

X-Ray Diffraction patterns of magnetite and cobalt doped magnetite via coprecipitation route have been shown in the above [figure 11](#). Characteristic peaks of magnetite can be observed for (200), (311), (440), (422), (511), and (440) at 30.3° , 35.6° , 41.4° , 53.5° , 57.4° , and 62.9° respectively. These are in accordance with standard JCPD card [01-088-0315] showing miller indices (220), (311), (400), (422), (511) and (440) at 2θ value of 30.2° , 35.5° , 43.2° , 53.5° , 57.2° , 62.7° proving the formation of inverse cubic spinal structure of magnetite. The same peaks have been observed for the cobalt doped but at slight receding angles. This has been depicted in [table 3](#). This is a common behavior shown by doped nanoparticles as the peaks shift slightly either right or left. This is due to the replacement of iron atoms by cobalt atoms at lattice points [\[36, 37\]](#).

Table 3: Comparison of 2θ degrees between Fe_3O_4 and $\text{Co}_{0.7}\text{Fe}_{2.3}\text{O}_4$ at same miller indices

Miller Indices (hkl)	Fe_3O_4	$\text{Co}_{0.7}\text{Fe}_{2.3}\text{O}_4$
(220)	30.3°	28.9°
(311)	35.6°	32.5°
(222)	-	37.5°
(440)	41.4°	41.4°
(422)	53.5°	47.3°
(511)	57.4°	55.0°
(400)	62.9°	62.0°

5.2 Scanning Electron Microscopy (SEM)

5.2.1 Fe_3O_4

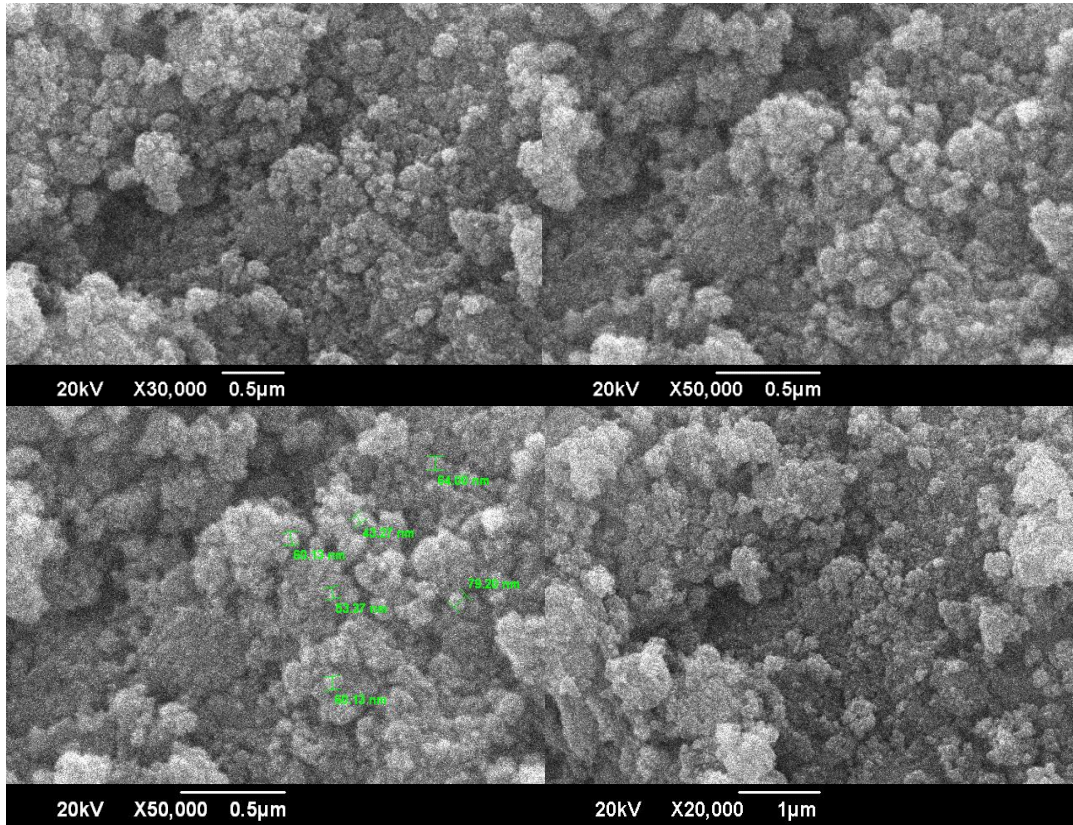


Figure 12: SEM images of Fe_3O_4 at different magnifications prepared by co-precipitation method

[Figure 12](#) shows the Scanning Electron Microscopy images of magnetite nanoparticles at different magnifications. First, the nanoparticles were dried in the drying oven to remove moisture. Then a small quantity of sample was added on a SEM tape after which a 400 Å gold layer was sputter coated on it in a sputter coating chamber to make it conductive. SEM images show formation of nanoparticles in nanometer range with spherical morphology. The size of nanoparticles is less than 100 nm though there is a wide distribution in size. Moreover, it can be observed that nanoparticles are in the state of high agglomeration and aggregation [\[38\]](#). This is because nanoparticles have a high surface to volume ratio. It leads to high surface energy which tends to bind the nanoparticles together. In addition to this phenomenon, small magnetic nanoparticles also agglomerate because of the dipole interactions and magnetic attraction [\[39\]](#). Images were taken on different magnifications such as 50,000 times, 30,000 times, and 20,000 times. The sole reason is to focus on the sample so that the sizes can be measured as precisely as possible.

5.2.2 $\text{Co}_{0.7}\text{Fe}_{2.3}\text{O}_4$

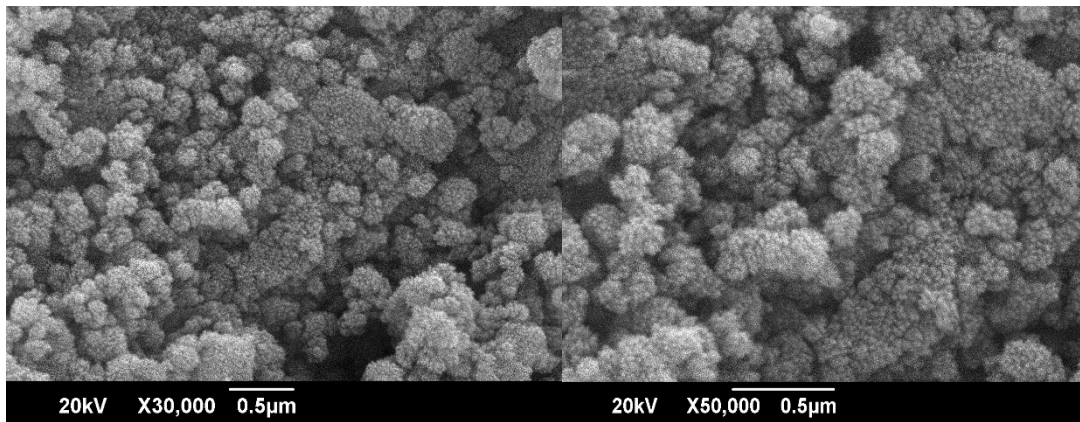


Figure 13: SEM images of $\text{Co}_{0.7}\text{Fe}_{2.3}\text{O}_4$ at different magnifications prepared by co-precipitation method

[Figure 13](#) shows the SEM images of Cobalt doped magnetite nanoparticles. Compared with the pure Magnetite nanoparticles, they have many similarities as well as some differences. First, agglomeration and aggregation can be seen due to high surface to volume ratio, dipole interactions and magnetic attraction between nanoparticles. Coming to differences, these nanoparticles look more refined than the Magnetite nanoparticles. This may be

because of the separate protocol that was used to synthesize these nanoparticles. 30,000 times and 50,000 times magnification have been used to focus more on the nanoparticles and to visualize them as best as possible.

5.4 Energy Dispersive X-Ray (EDX)

5.4.1 Fe₃O₄

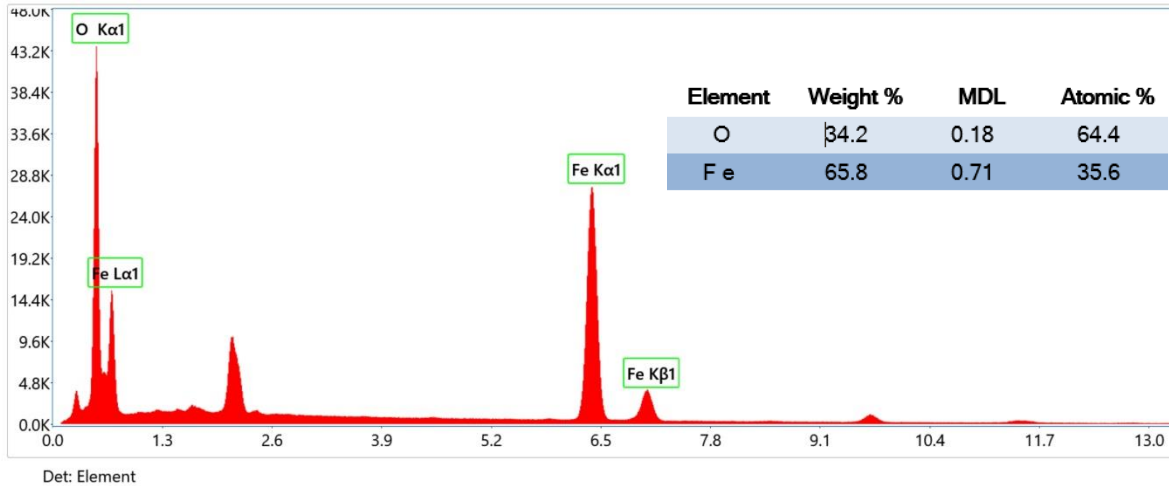


Figure 14: EDX graph of Fe₃O₄ prepared by co-precipitation method

[Figure 14](#) shows the EDX analysis of magnetite nanoparticles. In this qualitative and quantitative analysis, the atomic percent ratio of Oxygen to Iron is 1.8 though the atomic percent of Magnetite (Fe₃O₄) is 1.3. This deviation is due to the difference between theoretical and experimental ratios and generally, around 1.8 ratio is observed whenever Magnetite is synthesized. It is to be noted that this deviation does not alter the properties of Magnetite. On the other hand, the weight percent of Iron is greater than that of Oxygen. This is due to the fact that Iron is a heavier element than Oxygen. The peaks of both Iron and Oxygen are very prominent in the graph showing the purity of the sample.

5.4.2 Co_{0.7}Fe_{2.3}O₄

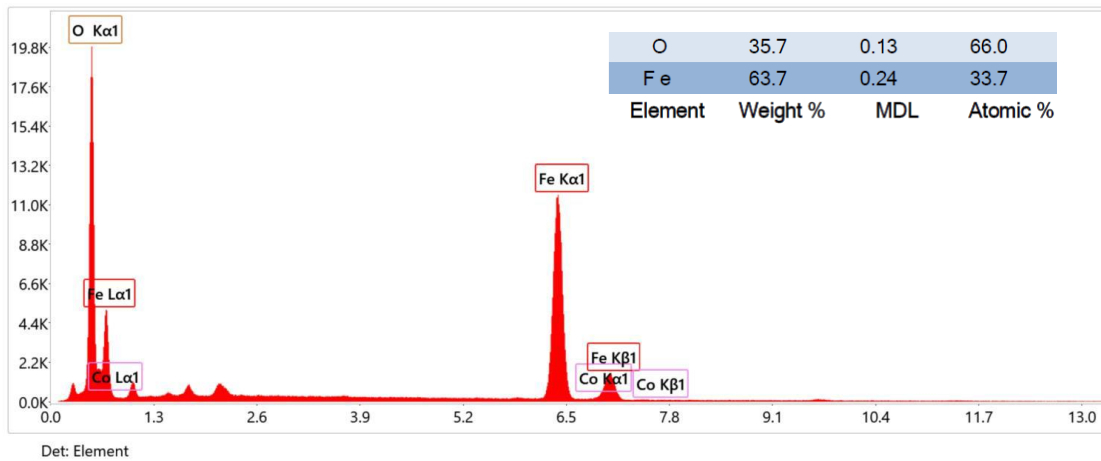


Figure 15: EDX graph of Co_{0.7}Fe_{2.3}O₄ prepared by co-precipitation method

[Figure 15](#) shows the EDX analysis of Cobalt doped Magnetite nanoparticles. It can be observed that Oxygen and Iron peaks can be seen having 66% atomic percent and 33.7% atomic percent, respectively. The atomic percent ratio between Oxygen and Iron comes out to be 1.95 which is the experimental ratio and differs from the theoretical ratio Magnetite (Fe₃O₄). This difference is generally seen whenever Magnetite is synthesized. In addition to this, a small Cobalt peak can also be seen which has an atomic percent of 0.3. If we compare this with the theoretical atomic percent of theoretical formula of Co_{0.7}Fe_{2.3}O₄, it is less which shows the experimental deviation which is seen frequently in literature. The weight percent of Iron is more than that of Oxygen because it is heavier. The weight percent of Cobalt is less because it is minute in amount.

5.3 Fourier-Transform Infrared Spectroscopy (FTIR)

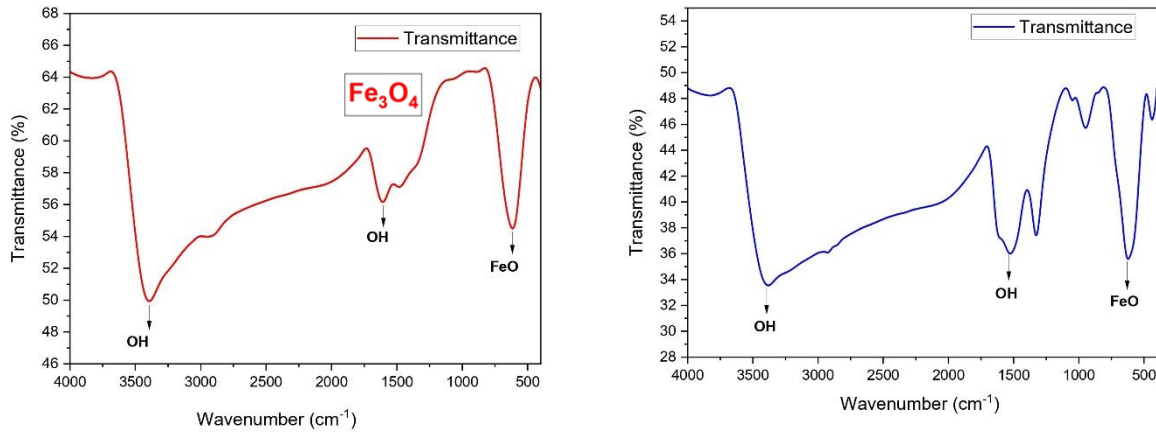


Figure 16: FTIR graphs of Fe_3O_4 (left) and $\text{Co}_{0.7}\text{Fe}_{2.3}\text{O}_4$ (right) prepared by co-precipitation method

[Figure 16](#) shows the Fourier-Transform Infrared Spectroscopy (FTIR) graphs of Magnetite and Cobalt doped magnetite nanoparticles. In the left graph, the signatures crusts and troughs of pure Magnetite can be observed. Fe–O trough indicates the stretching vibration mode of Iron and Oxygen atoms. Hydroxyl bonds (O–H) at 1500 cm^{-1} and 3500 cm^{-1} show the bending vibration mode and stretching vibration modes, respectively.

In the right graph, the crusts and troughs for Metal Oxide bond (Fe–O) and the Hydroxyl (O–H) bonds appear to be similar to pure Magnetite graph. However, there is a shift in this trough from 610 cm^{-1} to 632 cm^{-1} . This happens because of the fact that by doping a small quantity of Cobalt in Magnetite, it strengthens the Metal Oxide bond (Fe–O) in the Magnetite inverse cubic spinel lattice [\[40\]](#). This shifting indication confirms that the doping has been achieved. Hydroxyl bonds (O–H) show the bending vibrations and stretching vibrations at 1500 cm^{-1} and 3500 cm^{-1} , respectively which is same as that of Magnetite nanoparticles.

5.5 Time-Temperature Analysis

Time-Temperature analysis was conducted in Probe Sonicator to measure the temperature increase with respect to time for four samples as shown in [table 4](#). The are (1) De-ionized water and Cobalt doped magnetite nanoparticles, (2) De-ionized water, Cobalt doped magnetite nanoparticles and Bacteria (3) De-ionized water, cobalt doped magnetite nanoparticles and Rose Bengal (4) De-ionized water, Cobalt doped magnetite nanoparticles, Rose Bengal and Bacteria. As this is in vitro testing, bacteria were chosen to observe the temperature elevation behavior in it. The amounts of each material are also shown in [table 4](#). For both Magnetite and Cobalt doped magnetite nanoparticles, the amount was 0.03 g and for de-ionized water, the amount was 20mL. The amount of bacteria was 5 mL. These amounts remained the same for all the samples.

Table 4: Materials and amounts for Time-Temperature Analysis

Samples		Amounts
De-ionized water	+	DI water: 20 ml
Co_{0.7}Fe₃O₄ nanoparticles		NPs: 0.03 g
De-ionized water	+	DI water: 20 ml
Co_{0.7}Fe₃O₄ nanoparticles	+	NPs: 0.03 g
Bacteria		Bac: 5 ml
De-ionized water	+	DI water: 20 ml
Co_{0.7}Fe₃O₄ nanoparticles	+	NPs: 0.03 g
Rose Bengal		RB: 0.03 g
De-ionized water	+	DI water: 20 ml
Co_{0.7}Fe₃O₄ nanoparticles	+	NPs: 0.03 g
Bacteria		Bac: 5 ml
Rose Bengal		RB: 0.03 g

Before initiation of the analysis, some important specifications were set in the Probe Sonicator. The specifications are shown in [table 5](#). The process time was set 10 minutes per

cycle as per the literature. Pulse time on and off was set to 0.7 s and 0.3 respectively as shown in literature. Power rate was optimized to 60% to get the maximum temperature increase. The frequency of ultrasound was 25 kHz which was a built-in feature in the Probe Sonicator. These specifications were kept the same throughout the analysis.

Table 5: Probe Sonication specifications

Parameter	Value
Process time	10 minutes per cycle
Pulse ON	0.7 seconds
Pulse OFF	0.3 seconds
Alarm temperature	57°C
Probe temperature	Varying
Power rate	60 %
Ultrasound Frequency	25 kHz

[Figure 17](#) shows the time-temperature curve for all four samples. The initial temperature was kept to 26°C. It is observed that after pulsed ultrasound exposure of 10 minutes, all four samples experienced a temperature increased to 37°C, an 11°C rise. This shows the temperature increasing ability of magnetic nanoparticles in short amount of time. The analysis also shows that the addition of bacteria and Rose Bengal did not hinder the temperature elevation rate. This is because the ultrasounds got attenuated and scattered from the surface of Magnetic nanoparticles throughout the sample and it was not affected by other substances present.

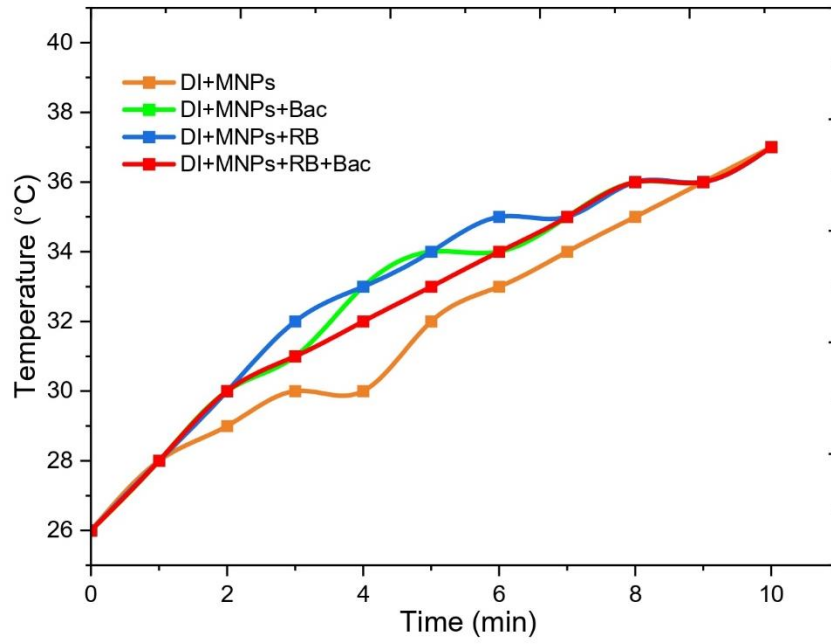


Figure 17: Time-Temperature graph of different combinations of materials

CONCLUSION

In this study, magnetite nanoparticles were synthesized using co-precipitation route. Secondly, Cobalt was doped in the magnetite nanoparticles to enhance the magnetization properties. This was confirmed from different experimental techniques which includes X-ray Diffraction, Scanning Electron Microscopy, Energy-Dispersive Spectroscopy and Fourier-Transform Infrared Spectroscopy. Then time-temperature analysis was performed on four samples, and we get a change in temperature from 26°C to 37°C resulting in rise of 11°C. This is evidence that all samples have the same rise which will give a synergistic effect. Finally, we additionally design a setup apart from our project objectives and we are planning to conduct more in vitro testing in the future to study the effect of interaction between ultrasounds and the cobalt doped magnetite nanoparticles.

FUTURE PLANS

Ultrasonic Hyperthermia Setup

After the project objectives were completed, it was decided to extend the scope and design a setup that is portable, which converges to real life application and to be used to study the interaction between ultrasounds and nanoparticles more effectively.

Material Procurement and Dimensions

The material used to make the setup was Acrylic which is a transparent, lightweight, stiff and strong plastic. It is the most suitable material for the setup because it is important to see through so that the process can be observed clearly from outside. It needs to be lightweight so that it can be moved from one place to another easily. It also needs to be stiff and strong so that the water pressure inside can be sustained. Furthermore, to prevent leakage, Silicone sealant was applied on all sides of the acrylic container. All items were procured from a local shop in Saddar, Rawalpindi.

[Figure 18](#) shows the Ultrasonic Hyperthermia setup from literature [\[16\]](#) and [Figure 19](#) shows the setup that we designed. The overall dimension of the setup is 20 cm x 20 cm x 20 cm. The length of the platform in the middle of the container at each side is 20 cm and width of 6.5 cm.

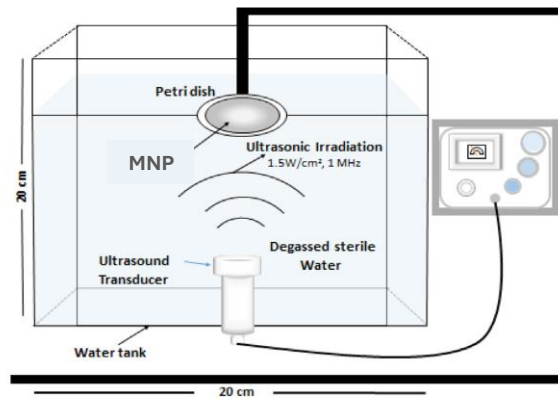


Figure 18: UHT Setup from literature [\[16\]](#)

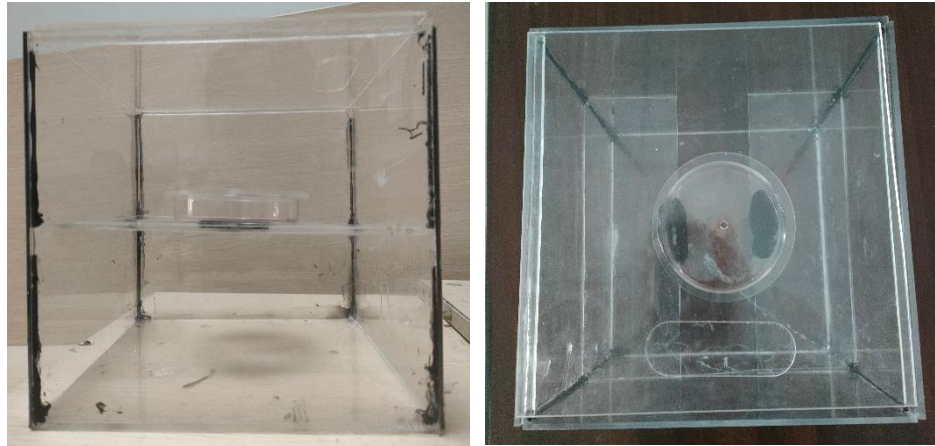


Figure 19: Self-designed UHT Setup Front view (left), Top view (right)

First nanomaterials and de-ionized water are added to the attached petri dish on a built platform in the container. It is then sealed with an acrylic covering. Through a hole in acrylic covering, one end of a thermocouple is added, and the other end is extended towards the outside of the container. The hole is sealed with Silicon sealant. The container is filled with water with an immersible transducer in it facing the top of the petri dish. Ultrasounds travels through the water and reaches the petri dish. Once they cross the petri dish, they interact with nanomaterial inside it. Due to ultrasound attenuation and scattering, heat is generated which is detected and measured by thermocouple. In this way, the temperature increase is measured using Ultrasonic Hyperthermia Setup.

It is important that no air should be present in the petri dish because it increases the impedance mismatch. In this case, ultrasounds get bounced back as it enters the petri dish and does not get scattered and attenuated at Magnetic nanoparticles which prevents temperature increase.

REFERENCES

1. Tiago P. Ribeiro, J. Agostinho Moreira, Fernando J. Monteiro, Marta S. Laranjeira, Nanomaterials in cancer: Reviewing the combination of hyperthermia and triggered chemotherapy, (2022) 1-15, <https://doi.org/10.1016/j.jconrel.2022.04.045>
2. L. T. H. Phong, D. H. Manh, P. H. Nam, V. D. Lam, B. X. Khuyen, B. S. Tung, T. N. Bach, D. K. Tung, N. X. Phuc, T. V. Hung, Thi Ly Mai, The-Long Phanf and Manh Huong Phan, Royal Society of Chemsitry, (2021), <https://doi.org/10.1039/D1RA07407E>.
3. Weinberg, Robert A. "How Cancer Arises." Scientific American 275, no. 3 (1996): 62–70. <http://www.jstor.org/stable/24993349>.
4. John C. Bailar, M.D., Ph.D., and Heather L. Gornik, M.H.S, Cancer Undefeated 1997), The New England Journal of Medicine, VOL. 336 NO. 22, DOI: 10.1056/NEJM199705293362206
5. Prof Ian F Tannock, FRCPC, Conventional cancer therapy: promise broken or promise delayed? (1998), THE LANCET SUPPLEMENT| VOLUME 351, SPECIAL ISSUE, SII9-SII16, [https://doi.org/10.1016/S0140-6736\(98\)90327-0](https://doi.org/10.1016/S0140-6736(98)90327-0)
6. Peter Nygren, What is cancer chemotherapy (2009), <https://doi.org/10.1080/02841860151116204>
7. Christine Allen, Sohyoung Her, David A Jaffray, Radiotherapy for Cancer: Present and Future (2017), <https://doi.org/10.1016/j.addr.2017.01.004>
8. Lynda Wyld, Riccardo A. Audisio & Graeme J. Poston, The evolution of cancer surgery and future perspectives (2014), <https://doi.org/10.1038/nrclinonc.2014.191>
9. X. Liang, J. Gao, L. Jiang, J. Luo, L. Jing, X. Li, Y. Jin, Z. Dai, Nanohybrid Liposomal Cerasomes with Good Physiological Stability and Rapid Temperature Responsiveness for High Intensity Focused Ultrasound Triggered Local Chemotherapy of Cancer, (2015) 1-52, <https://doi.org/10.1021/nn507482w>.
10. J. Beik, Z. Abed, A. Ghadimi-Daresajini, M. Nourbakhsh, A. Shakeri-Zadeh, M. S. Ghasemi, M.B. Shiran, Measurements of nanoparticle-enhanced heating from 1 MHz ultrasound in solution and in mice bearing CT26 colon tumors, J. Therm. Biol. 62 (2016) 1-6 <https://doi.org/10.1016/j.jtherbio.2016.10.007>.

11. Y.W. Chen, T.Y. Liu, P.H. Chang, P.H. Hsu, H.L. Liu, H.C. Lin, S.Y. Chen, A theranostic nrGO@MSN-ION nanocarrier developed to enhance the combination effect of sonodynamic therapy and ultrasound hyperthermia for treating tumor, *Nanoscale*. 8 (2016) 1-10, <https://doi.org/10.1039/c5nr07782f>.
12. Z. Deng, Y. Xiao, M. Pan, F. Li, W. Duan, L. Meng, X. Liu, F. Yan, H. Zheng, Hyperthermia- triggered drug delivery from iRGD-modified temperature-sensitive liposomes enhances the anti- tumor efficacy using high intensity focused ultrasound, *J. Control. Release* 243 (2016) 1-27, <https://doi.org/10.1016/j.jconrel.2016.10.030>.
13. J. Beik, M.B. Shiran, Z. Abed, I. Shiri, A. Ghadimi-Daresajini, F. Farkhondeh, H. Ghaznavi, A. Shakeri-Zadeh, Gold nanoparticle-induced Sono sensitization enhances the antitumor activity of ultrasound in colon tumor-bearing mice, *Med. Phys.* 45 (2018) 1-27, <https://doi.org/10.1002/mp.13100>.
14. R. Irajirad, A. Ahmadi, B.K. Najafabad, Z. Abed, R. Sheervalilou, S. Khoei, M. B. Shiran, H. Ghaznavi, A. Shakeri-Zadeh, combined thermo-chemotherapy of cancer using 1 MHz ultrasound waves and a cisplatin-loaded Sono sensitizing nanoplatform: an in vivo study, *Cancer Chemotherapy. Pharmacol.* 84 (2019) 1-7, <https://doi.org/10.1007/s00280-019-03961-9>.
15. C.J. Th´ebault, G. Ramniceanu, S. Boumati, A. Michel, J. Seguin, B. Larrat, N. Mignet, C. M´enager, B.T. Doan, Theranostic MRI liposomes for magnetic targeting and ultrasound triggered release of the antivasular, CA4P, *J.Control. Release* 322 (2020), 1-12, <https://doi.org/10.1016/j.jconrel.2020.03.003>.
16. T. Shalaby, A. Gawish, H. Hamad, A Promising Platform of Magnetic Nanofluid and Ultrasonic Treatment for Cancer Hyperthermia Therapy: In Vitro and in Vivo Study, *Ultrasound Med. Biol.* 47 (2021) 1-15, <https://doi.org/10.1016/j.ultrasmedbio.2020.11.023>
17. Taebin Ahn, Jong Hun Kim, Hee-Man Yang, Jeong Woo Lee, and Jong-Duk Kim, Formation Pathways of Magnetite Nanoparticles by Coprecipitation Method (2012), American Chemical Society, <https://doi.org/10.1021/jp211843g>
18. George W. Morey, Hydrothermal Synthesis (1953), *Journal of the American Ceramic Society*, <https://doi.org/10.1111/j.1151-2916.1953.tb12883.x>

19. J. Livage, C. Sanchez, Sol-gel chemistry (1992), Journal of Non-Crystalline solids, [https://doi.org/10.1016/S0022-3093\(05\)80422-3](https://doi.org/10.1016/S0022-3093(05)80422-3)
20. K. Petcharoen, A. Sirivat, Synthesis and characterization of magnetite nanoparticles via the chemical co-precipitation method (2012), <https://doi.org/10.1016/j.mseb.2012.01.003>
21. Safia Anjum, Rabia Tufail, Khalid Rashid, Rehana Zia, S. Riaz, Effect of cobalt doping on crystallinity, stability, magnetic and optical properties of magnetic iron oxide nanoparticles (2017), Journal of Magnetism and Magnetic Materials, <http://dx.doi.org/10.1016/j.jmmm.2017.02.006>
22. I P T Indrayana, L A Tjuana¹, M T Tuny and Kurnia, Nanostructure and Optical Properties of Fe₃O₄: Effect of Calcination Temperature and Dwelling Time (2019), Journal of Physics: Conference Series, doi:10.1088/1742-6596/1341/8/082044
23. Robert Schlögl, Chapter 5 X-ray Diffraction: A Basic Tool for Characterization of Solid Catalysts in the Working State (2009), Advances in Catalysis, [https://doi.org/10.1016/S0360-0564\(08\)00005-9](https://doi.org/10.1016/S0360-0564(08)00005-9)
24. J. Epp, 4 - X-ray diffraction (XRD) techniques for materials characterization (2016), Materials Characterization using Nondestructive Methods, <https://doi.org/10.1016/B978-0-08-100040-3.00004-3>
25. C. Zhao, B. Wang, S. Zhong, Md. Akhtaruzzaman, W. Lang, H. Chen, Chapter 12 - NDT studies of nanoscale polymeric coatings (2023), Polymer-Based Nanoscale Materials for Surface Coatings, <https://doi.org/10.1016/B978-0-32-390778-1.00019-0>
26. Siti Fatimah, Risti Ragadhita, Dwi Fitria Al Husaeni, Asep Bayu Dani Nandiyanto, How to Calculate Crystallite Size from X-Ray Diffraction (XRD) using Scherrer Method (2022), ASEAN Journal of Science and Engineering, <http://dx.doi.org/10.2017509/xxxxt.vxix>
27. H. J. Leamy, Charge collection scanning electron microscopy (1982), Journal of Applied Physics, <https://doi.org/10.1063/1.331667>
28. K.D. Vernon-Parry, Scanning electron microscopy: an introduction (2000), [https://doi.org/10.1016/S0961-1290\(00\)80006-X](https://doi.org/10.1016/S0961-1290(00)80006-X)

29. B.J. Inkson, 2 - Scanning electron microscopy (SEM) and transmission electron microscopy (TEM) for materials characterization (2016), Materials Characterization Using Nondestructive Evaluation (NDE) Methods, <https://doi.org/10.1016/B978-0-08-100040-3.00002-X>
30. Prof. Dr. Gernot Friedbacher, Dr. Henning Bubert, Surface and Thin Film Analysis: A Compendium of Principles, Instrumentation, and Applications (2011), DOI:10.1002/9783527636921
31. Raghvendra Kumar Mishra, Ajesh K. Zachariah, Sabu Thomas, Chapter 12 - Energy-Dispersive X-ray Spectroscopy Techniques for Nanomaterial (2017), <https://doi.org/10.1016/B978-0-323-46141-2.00012-2>
32. Manuel Scimeca, Simone Bischetti, Harpreet Kaur Lamsira, Rita Bonfiglio, and Elena Bonanno, Energy Dispersive X-ray (EDX) microanalysis: A powerful tool in biomedical research and diagnosis (2018), <https://doi.org/10.4081%2Fejh.2018.2841>
33. Catherine Berthomieu, Rainer Hienerwadel, Fourier transform infrared (FTIR) spectroscopy (2009), DOI 10.1007/s11120-009-9439-x
34. Aastha Dutta, Chapter 4 - Fourier Transform Infrared Spectroscopy (2017), Micro and Nano Technologies, <https://doi.org/10.1016/B978-0-323-46140-5.00004-2>
35. R.R. Retamal Marín, F. Babick, M. Stintz, Ultrasonic dispersion of nanostructured materials with probe sonication – practical aspects of sample preparation (2017), Powder Technology, <https://doi.org/10.1016/j.powtec.2017.05.049>
36. T. Truc, N. Hoan, D. Bach, T. Thuy, K. Ramadass, C. Sathish, N. Chinh, N. Trinh, T. Hoang, Hydrothermal Synthesis of Cobalt Doped Magnetite Nanoparticles for Corrosion Protection of Epoxy Coated Reinforced Steel (2020), Journal of Nanoscience and Nanotechnology, doi: 10.1166/jnn.2020.17413
37. S. Anjum, R. Tufail, H. Saleem, R. Zia, S. Riaz, Investigation of Stability and Magnetic Properties of Ni- and Co-Doped Iron Oxide Nanoparticles (2017), DOI 10.1007/s10948-017-4044-2
38. Dieter Vollath, Agglomerates of nanoparticles (2020), Beilstein Journal of Nanotechnology, <https://doi.org/10.3762/bjnano.11.70>

- 39.** Eldin Wee Chuan Lim, Ruili Feng, Agglomeration of magnetic nanoparticles (2012), The Journal of Chemical Physics, <https://doi.org/10.1063/1.3697865>
- 40.** Hassan Soleimani, Noor Rasyada Ahmad Latiff, Hasnah Mohd Zaid, Noorhana Yahya, Amir R. Sadrolhosseini, Muhammad Adil, Influence of cobalt substitution on the structural and magnetic properties of cobalt substituted magnetite (2016), American Institute of Physics, <http://dx.doi.org/10.1063/1.496s>